Manufacturing time estimator based on kinematic and thermal considerations: application to WAAM process

Ricardo Viola, Fabien Poulhaon, Xavier Balandraud, Pierre Michaud, Emmanuel Duc

Manufacturing time estimator based on kinematic and thermal considerations: application to WAAM process

Ricardo VIOLA[a,b], Fabien POULHAON[b], Xavier BALANDRAUD[a], Pierre MICHAUD[b], Emmanuel DUC[a]

(a) Clermont Auvergne INP, Université Clermont Auvergne, CNRS, Institut Pascal, 63000 Clermont-Ferrand, France Mail : r.viola@estia.fr

(b) Université Bordeaux, ESTIA Institute of Technology, F-64210 Bidart, France

Abstract: Metal additive manufacturing (AM) has been pointed as the answer to reduce manufacturing time and cost for aeronautic parts with a high buy to fly ratio. The manufacturability of a part by AM depends on important indicators that would allow it to be cost effective. One important indicator is the manufacturing time which is highly dependent on an important factor: the interlayer time. The interlayer time is the time needed by the material to cool down to a temperature, called interlayer temperature, that allows a new deposition of molten material. The interlayer temperature is intimately correlated with the cooling curve of the material. It is defined using time-temperature-transformation (TTT) diagrams. The final goal is to avoid the appearance of detrimental phases that could lead to a decrease in the material's mechanical properties. The difficulty of predicting the cooling time is due to the influence of the part geometry, the deposition strategy, and the dimensions of the substrate. Their correlation also needs to be understood in order to minimize the deposition time (Dt) while ensuring an acceptable material quality. This paper presents a methodology to estimate manufacturing time that combines kinematic and thermal criteria for Wire and Arc Additive Manufacturing (WAAM) process. Application was performed for stainless steel 316L. In this first step toward an advanced manufacturing time estimator, only the first layer attached to the building plate is analyzed from a thermal point of view. The thermal analysis is based on an analytical model enabling the evaluation of the preheating temperature (PhT) in a first approach and providing an adequate framework for the evaluation of cooling curves in a second time. It includes an accurate description of robot kinematics through the consideration of a realistic travel speed evolution along

the toolpath. This model is used to evaluate through an indicator that quantifies the thermal influence of a given deposition strategy. The results show the dependency relationship between manufacturing strategy and inherent thermal gradient and its implications on part production time.

Key words: Trajectory, Thermal model, Manufacturing-Time, Process-Indicator.

1 Introduction

Additive manufacturing of metals has brought new development and optimization perspectives for part geometries and production processes especially for parts with large dimensions (Cunningham *et al.*, 2018). The greater design freedom is due to its layered production mode. The fact that the CAD model is sectioned by layers (called slicing) brings many advantages, but also some challenges when it comes to toolpath programming (Wu *et al.*, 2018). The metal deposition trajectory for each layer must be carefully planned. The planning of each layer must obey several rules imposed by the geometry of the part to build, by the material to be used, or even by the very process with which it will be manufactured.

Some of the essential conditions imposed by the material are related to the overlap, as well as to the temperatures to which the material is exposed during certain periods of time while manufacturing the part (Jin *et al.*, 2020). Currently, the trajectories used in the robotized WAAM process are limited by the number of stops, the overlap between layers, and also radius of curvature used (Ding *et al.*, 2014). These limitations are related to the robot's kinematics and the existing system between cold metal transfer (CMT) equipment and robot controller (Viola et al, 2021). Most of the methods used nowadays to define toolpath do not take into account the pre-requisites of the material to obtain a part with the best mechanical properties possible for this production process.

Each material deposition strategy has a direct influence on how the heat is distributed over the workpiece leading to the appearance of heat concentration points along the toolpath (Diourté, 2021). These heat concentration points might lead to locally different cooling kinetics and therefore to potentially different material microstructure and properties. Indeed, specific phase transformations may occur when the material is subjected to specific ranges of temperatures during certain periods of time (depending on the material used) (Geng *et al.*, 2017). The prediction and the anticipation of "hot points" is therefore of great interest in the design of an optimized toolpath.

Moreover, thermal gradient to which the workpiece under construction is subjected is known to be one of the driving causes for stress, plastic strain, and distortion (Mukin *et al.*, 2021). Heat dissipation during the WAAM process plays an important role, since this is intrinsically related to its productivity. The appearance of heat concentration points in the toolpath, is the result of the deposition strategy adopted (Mukin, Valdaytseva and Turichin, 2021). These points with very lower cooling speeds, negatively affect the productivity of the process when it is intended to comply with the interlayer temperatures designated by the manufacturer of the metallic material to be deposited (Mohebbi, Kühl and Ploshikhin, 2020). The toolpath of each layer must then be programmed considering the heat conduction between the various points on the part, thus achieving a lower thermal gradient across the part (Li and Xiong, 2019).

Thermal simulation based on Finite Element Method (FEM) is one of the most natural approaches for studying the thermal impact of a given toolpath (Ren *et al.*, 2020). Nevertheless, due to the complexity of these models, programming and parameterization requires specialized human resources. In addition, the calculation time associated with FEM simulation limits its use to small size components (Wolfer *et al.*, 2019), causing it not to be suited to an optimization loop where several deposition strategies need to be simulated (Li *et al.*, 2021).

The search for an alternative to standard FEM simulation is at the core of several developments. The use of analytical or semi-analytical models is one possible option. Rosenthal model enables to derive the temperature field in the cross section of a weld and is particularly well adapted to the estimation of the melt-pool size, and the heat affected zone (Nunes, 1983). Other approaches based on superposition of instant point sources, or flash method based are presented in (Ettaieb, Lavernhe and Tournier, 2021).

The objective of this work is to propose an alternative to FEM, making possible the comparison of several deposition strategies in a reasonable amount of time. For that purpose, a model inspired from welding was considered. It aims to introduce in a simple and clear form, thermal concepts to be taken into account when programming a trajectory for the production of large parts. Four different strategies are addressed, and the model is then compared to conventional FEM simulation results considered as reference data.

2 Motivation

In order to be able to make a precise comparison between the manufacturing process of a part using WAAM and other so-called standard processes, it is necessary to create a techno-economic model. This techno-economic model is actually the result of an evaluation of the productivity of the WAAM process.

The suitability of a process for producing certain parts is determined by several factors. The most relevant factors are the productivity of the process, the cost per part, and the quality of the part considering the same part design. Taking these concepts into account, making a productivity estimate becomes essential for building a technical-economic model. To that end, a reliable estimation of manufacturing time is a key point and must be addressed from both a kinematic point of view but also from a thermal point of view.

Indeed, the introduction of interlayer times directly affects the productivity. These interlayer times are actually the time required for the temperature of the deposited material to decrease, which can be quite long. The purpose of the interlayer time is to make sure that the deposition of each layer is done under similar thermal conditions, thus achieving the same microstructures and mechanical properties throughout the part. But the interlayer time is also dependent on the trajectory used. The role that the trajectory plays is critical, not only from a kinematic point of view, but also from a thermal point of view in the distribution of heat during the construction of the part. The use of a "light" model to simulate the influence of each path on the WAAM process is therefore of utmost importance.

3 Thermo-kinematic model

3.1 Assumptions made for the thermo-kinematic model

The proposed model has in consideration the following assumptions:

- Heat conduction is considered to be the driving cause for temperature rise in the part, convection and radiation at the boundaries are omitted.
- Thermal properties of material are considered uniform.
- The analytical model is based on semi-infinite domain approximation, meaning that the substrate is supposed to be infinitely thick and without boundaries in X and Y axis.
- Mirror boundary conditions are applied at all edges to account for finite domain boundaries (i.e. to transform the model into a simulation closer to reality)

3.2 Analytical model for transient heat equation

Given the aforementioned assumptions, the solution to the transient heat equation that describes the evolution in time and space of the temperature in the manufactured part, can be analytically derived using a Green's function (Wolfer *et al.*, 2019) denoted as *G* and written as:

$$G(\boldsymbol{x}, t) = \frac{1}{(4\pi D t)^{\frac{3}{2}}} exp(-\frac{\|\boldsymbol{x}\|^2}{4Dt}) \quad (1)$$

Where $\boldsymbol{x} = (x, y, z)$ is a position in the 3D computational domain, t is the time and D is the thermal diffusivity of the material. By integrating G over a short period of time Δt, one can evaluate the temperature rise generated by an instant point source (Dirac) of amplitude 1, located at position **(**0, 0, 0), that would be active (and not moving) during that period Δt.

Considering a more generic source term $Q(x,t)$, and making use of the superposition principle, the temperature field is obtained with the following relation:

$$T(\boldsymbol{x}, t) = \int_0^t \int_\Omega G(\boldsymbol{x} - \boldsymbol{X}, t - \tau) \cdot Q(\boldsymbol{X}, \tau) d\boldsymbol{X} d\tau + \int_\Omega G(\boldsymbol{x} - \boldsymbol{X}, t) \cdot T(\boldsymbol{X}, 0)\ dX \quad (2)$$

Where $\boldsymbol{X} = (X, Y, Z)$ is again a position in the computational domain. Two contributions are summed up, the first one is associated to heat input and will be denoted T_{inp}. The second one is associated to heat diffusion in the absence of a heat source and will be denoted T_{dif}.

By considering a discretization of the time interval into timesteps $(t_i)_{i=1,n}$, the evolution of temperature is computed incrementally using the relation:

$$T(\boldsymbol{x}, t_i) = \int_{t_{i-1}}^{t_i} \int_\Omega G(\boldsymbol{x} - \boldsymbol{X}, t_i - \tau) \cdot Q(\boldsymbol{X}, \tau) d\boldsymbol{X} d\tau + \int_\Omega G(\boldsymbol{x} - \boldsymbol{X}, t_i - t_{i-1}) \cdot T(\boldsymbol{X}, t_{i-1})\ dX \quad (3)$$

This relation remains valid for any type of source term, acting on surface only or in the volume. In the case a double ellipsoid/Goldak heat source (see Figure 1), more suited to the description of heat input in WAAM process, the heat input contribution simplifies to the following integral over time:

$$T_{inp}(\boldsymbol{x}, t_i) = \frac{3\sqrt{3}Q}{2\rho c_p \pi\sqrt{\pi}} \int_{t_{i-1}}^{t_i} \left(\frac{A(\boldsymbol{x}, t_i)}{12D(t_i - \tau) + a_f^2} + \frac{B(\boldsymbol{x}, t_i)}{12D(t_i - \tau) + a_r^2} \right) \frac{d\tau}{\sqrt{(12D(t_i - \tau) + b^2)(12D(t_i - \tau) + c^2)}} \quad (4)$$

Where ρ and c_p are the density and the specific heat of the material, Q is the power, $A(\boldsymbol{x}, t_i)$ and $B(\boldsymbol{x}, t_i)$ are functions defined as follows:

$$A(\boldsymbol{x}, t_i) = r_f * \exp\left(-\frac{3\big(x - V(\tau - t_i)\big)^2}{12D(t_i - \tau) + a_f^2} - \frac{3y^2}{12D(t_i - \tau) + b^2} - \frac{3z^2}{12D(t_i - \tau) + c^2} \right) \quad (5)$$

$$B(\boldsymbol{x}, t_i) = r_r * \exp\left(-\frac{3\big(x - V(\tau - t_i)\big)^2}{12D(t_i - \tau) + a_r^2} - \frac{3y^2}{12D(t_i - \tau) + b^2} - \frac{3z^2}{12D(t_i - \tau) + c^2} \right) \quad (6)$$

with b the half-width, c the depth, a_f (resp. a_r) the length of the front (resp. rear) portion of the double ellipsoid, as shown on Figure 1. V is the travel speed of the heat source in the time interval (t_{i-1}, t_i), assuming a motion along the x-direction, r_f (resp. r_r) is the portion of power distributed in front (resp. rear) part of the double ellipsoid.

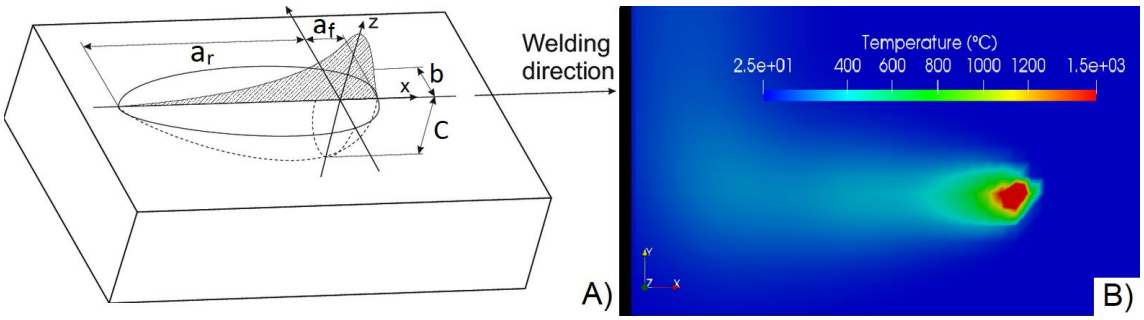

Figure 1 – A) Double ellipsoid (Lundbäck, 2022) B) Image of the moving heat source in the model

The interested reader can refer to (Nguyen *et al.*, 1999) for details about the calculation. The heat source contribution is relatively fast to compute and only needs to be evaluated in the vicinity of the source path. Indeed, one can notice that the previous relation can be split into two integrals over time with the integrand being a product of 1D Gaussian functions. The standard deviation of each gaussian function is an indication about the size of the zone affected by the heat source. As a result, considering a distance of 3 to 4 times the standard deviation in each direction around the heat source path is enough to evaluate its impact on temperature rise. The evaluation of the diffusion term is more time consuming since it requires several 3D integrations. An optimization of this calculation was not carried out in this work but is clearly identified as a key challenge to make the overall approach even more competitive from a computation time point of view.

4 Indicator

The presented indicator is only focused on the first layer deposed over the substrate. In study are the thermal conditions along the toolpath with regard to their thermal homogeneity or heterogeneity. So, in this context the *T* used in the indicator formula is the substrate temperature immediately prior to material deposition. Consequently, T_{max} is the maximum temperature that the substrate reaches immediately before material deposition along the entire length of the toolpath. The objective is to identify potential "hot points" along toolpath where the temperature is already high before reaching it with the heat source. A simple indicator, $I_{preheat}$ is defined as follows:

$$I_{preheat} = \left(\frac{T - T_0}{T_{max} - T_0}\right) \tag{7}$$

Where T_0 is the initial temperature of substrate, *T* is the PhT estimated with the model and T_{max} is an overall maximum temperature for a given strategy. T_{max} is defined after the entire thermal history of the substrate has been evaluated $I_{preheat}$ ranges therefore from 0 to 1. The indicators can be calculated in two configurations: one when the temperatures collected to build the scale is only from one strategy, called "Local indicator" (LI), and another where the temperatures collected to build the scale are from several strategies simulated and compared, named "Global indicator" (GI). In the first configuration T_{max} assumes the highest temperature from the only strategy simulated delivering an LI indicator. In the second configuration T_{max} assumes the highest value of temperature from all the strategies considered. The scale between 0 and 1 for GI despite being the same, is considering a different T_{max} if compared to LI's T_{max}. By doing so, the "thermal homogeneity" of each toolpath can be analyzed and an ideal strategy (from this indicator point of view) can be derived.

5 Study case

The study case consists of a series of simulations of linear segment deposition performed on top of a 200 x 200 x 5 (mm) substrate made of 316L stainless steel.

Table 1: Material properties of 316L stainless steel(J.J. Valencia et al., 2008)

k, thermal conductivity	15	[$W.m^{-1}.K^{-1}$]
c_p, specific heat capacity	470	[$J.kg^{-1}.K^{-1}$]
ρ, density	7800	[$kg.m^{-3}$]
D, thermal diffusivity	4	[$m^2.s^{-1}$]

The heat source is a double ellipsoid with an effective power (theorical power x efficiency) of 2000W (Q parameter in formula 4). Its geometrical parameters were kept constant over the time and are given in table 2. For the sake of simplicity, the heat source in our model is always considered constant, thus not taking into account the variation of power and WFS at arc ignition and extinction.

Table 2: Goldak geometric heat source parameters collected in Addimadour

af, front length	2	[mm]
ar, rear length	4	[mm]
b, half width	2	[mm]
c, depth	2	[mm]

The travel speed is set to 12mm/s during deposition and to 50mm/s during transition movements (TM), where the height considered was Z = 0.

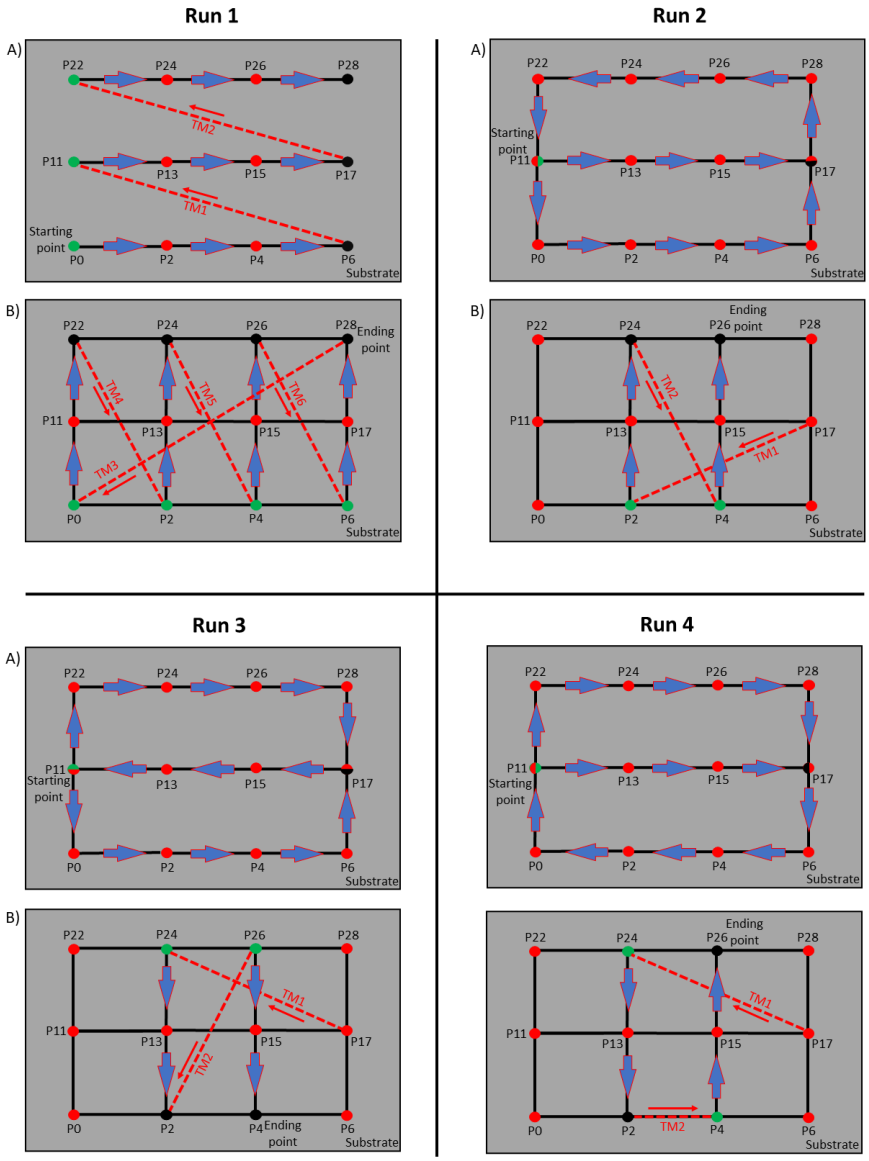

Figure 2 - Representation of the four strategies considered in this study Run 1, 2, 3, and 4, separated into A) and B) two phases of the same deposition strategy

Four different strategies are represented in Figure 2 with designations RUN 1, 2, 3 and 4. The green points mark the arc transition from arc OFF to arc ON. The black points mark the opposite transition from arc ON to arc OFF. The red points are intermediate points during a continuous movement that might contain speed variations. The points divided

into two halves with the colors red and black have a double meaning, they are intermediate points (half marked with red), and where there is a transition from on to off arc (half marked with black). The black lines are the simulated toolpaths, and the red discontinuous lines represent the transition movements (TM).
As far as the analytical model is concerned, the temperature field is evaluated on a grid made of a total of 23104 points 76x76x4. For comparison and validation purposes, the same grid is considered for building a 3D mesh necessary for the FEM reference simulations.

6 Results

Initially the local preheating indicator (LI) was evaluated for each strategy. In Figure 3 A) we can see the evolution of this indicator along the Run 1. Here T_{max} corresponds to the maximum PhT obtained over the entire Run 1. Figure 3 represents the comparison of results obtained between the model presented here 3 A) and the FEM simulation 3 B), showing that with the calibration performed the results obtained are consistent.
For the Run 1 here compared (Figure 3) the same trend is observed with both analytical and finite element model, as it can be seen by the identification of two "hot spots" in the vertical segments (top left side).

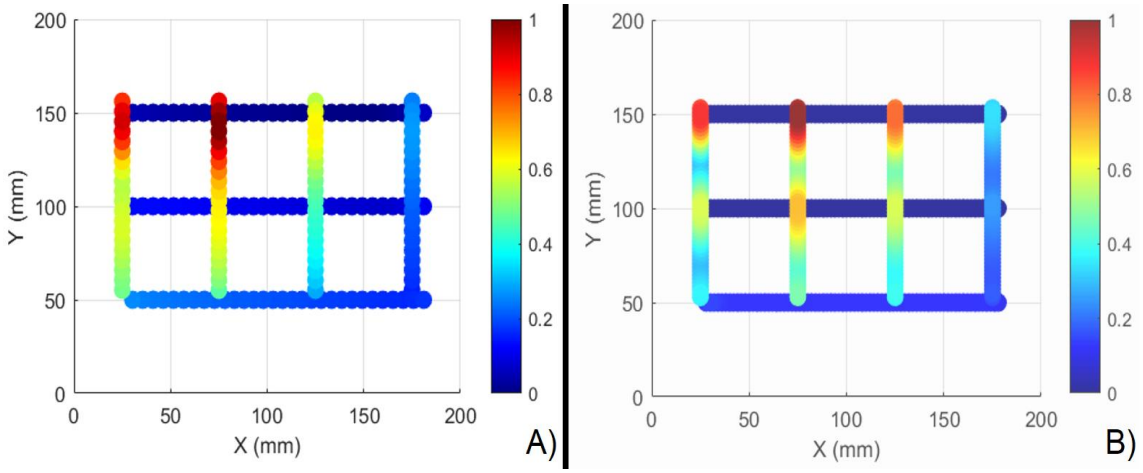

Figure 3 - Comparison of preheating indicator for strategy #1 evaluated with analytical model (A)) and FEM simulation (B))

Figure 4 shows the result of the GI indicators from the simulation done with the analytical model for the four strategies presented in Figure 2. Here the T_{max} considered (T_{max} corresponds to 1 on the scale) is the maximum temperature value reached on all four toolpaths. The lower indicator values (zero) are shown in a dark blue, meaning no preheating influence, this scale changes through a gradient of colors until the higher value 1 in dark red meaning that the points with this color have the higher preheating influence. Thus, in a simple and precise way, it allows to interpret the results visually.
Ranking in increasing order of the thermal influence that preheating has on the substrate, we have Run 1, Run 3, Run 4, and lastly Run 2. In Run 2 we can observe the existence of a hot point at the coordinate (x = 100, y = 75).

The fact that Run 1 has the smallest thermal gradient is logically consistent with its longest simulated Dt of 99.8s, which also has the longest toolpath length of 1682mm.

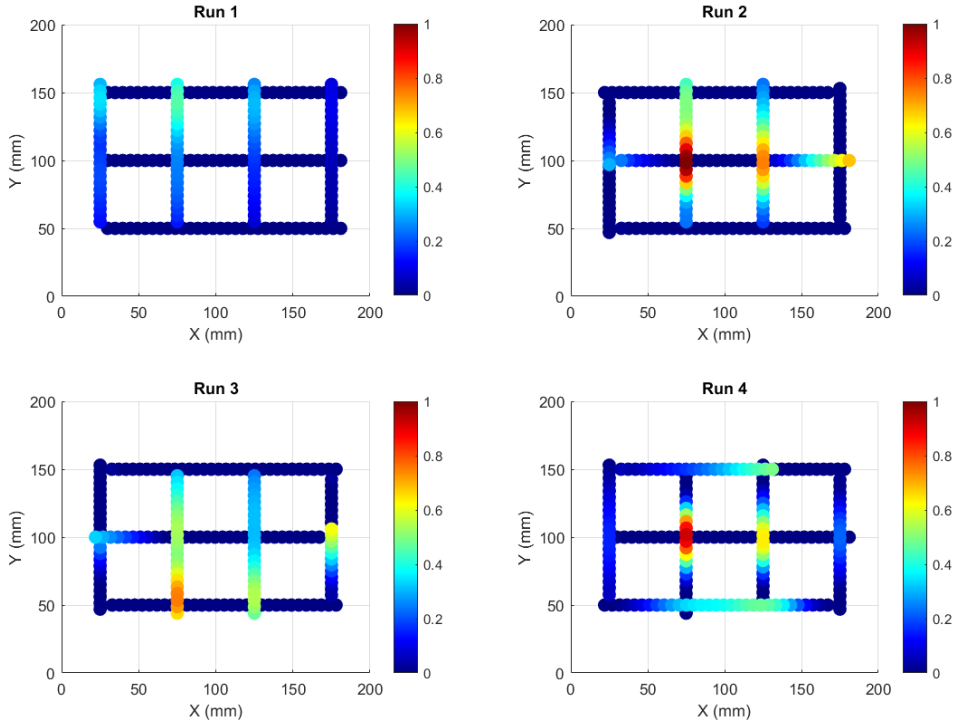

Figure 4 - Comparison of global preheating indicator (GI) for all strategies evaluated

The fact of being the longest trajectory allows the heat to be conducted through the substrate over a longer period, leading to lower indicator values for PhT in the vertical segments.

Run 2 and 3 have the same Dt of 80.7s for the same theoretical length (including both deposition and transition moves). Although theoretically we have equal Dt values for Run 2 and 3, the thermo-kinematic model tested here clearly represents that Run 3 undergoes a smaller thermal gradient across the part.

In the same way we can also see that the lower Dt of 79.4s in Run 4 with the shorter path length (1011.8 mm) does not necessarily mean a higher thermal gradient across the part. When comparing Run 4 with Run 2 it is possible to identify that Run 2 reaches higher GI for PhT at two points in its trajectory, and its cause is simply the trajectory chosen. The evaluation of preheating indicator required a computation time of around 10 to 12min for each strategy when using the thermo-kinematic model. This time rises to almost one hour per strategy studied in the case of FEM simulation. The use of the analytical model is thus of great interest as soon as the number of combinations to be tested is large.

7 Conclusions

The thermo-kinematic model proved to be faster and cheaper to compute compared to a full FEM simulation. The model allows to identify hot points along the trajectory and to select an optimal strategy based on thermal and material requisites. Such an optimal strategy doesn't necessarily correspond to the more efficient solution in terms of manufacturing time. The presented thermo-kinematic model can help selecting the best

compromise. The application of the model on larger components still requires an improvement in the evaluation of the diffusion contribution to the thermal field. This model provides a real estimate of the deposition time associated with a thermal behavior, allowing to adapt the interlayer times (if necessary) according to the existence of hot spots. Future work will focus on adapting the model to subsequent layers with the goal of achieving DT estimation for the entire part.

Acknowledgments This work is part of INDUSADDI project funded by the French Research Agency (ANR).

References

Cunningham, C.R. *et al.* (2018) 'Invited review article: Strategies and processes for high quality wire arc additive manufacturing', *Additive Manufacturing*, 22, pp. 672–686. Available at: https://doi.org/10.1016/j.addma.2018.06.020.

Ding, D. *et al.* (2014) 'A tool-path generation strategy for wire and arc additive manufacturing', *The International Journal of Advanced Manufacturing Technology*, 73(1–4), pp. 173–183. Available at: https://doi.org/10.1007/s00170-014-5808-5.

Diourté, A. (2021) 'Continuous three-dimensional path planning (CTPP) for complex thin parts with wire arc additive manufacturing', *Additive Manufacturing*, p. 15.

Ettaieb, K., Lavernhe, S. and Tournier, C. (2021) 'A flash-based thermal simulation of scanning paths in LPBF additive manufacturing', *Rapid Prototyping Journal*, 27(4), pp. 720–734. Available at: https://doi.org/10.1108/RPJ-04-2020-0086.

Geng, H. *et al.* (2017) 'Optimisation of interpass temperature and heat input for wire and arc additive manufacturing 5A06 aluminium alloy', *Science and Technology of Welding and Joining*, 22(6), pp. 472–483. Available at: https://doi.org/10.1080/13621718.2016.1259031.

Jin, W. *et al.* (2020) 'Wire Arc Additive Manufacturing of Stainless Steels: A Review', *Applied Sciences*, 10(5), p. 1563. Available at: https://doi.org/10.3390/app10051563.

Li, R. *et al.* (2021) 'Effect of path strategy on residual stress and distortion in laser and cold metal transfer hybrid additive manufacturing', *Additive Manufacturing*, 46, p. 102203. Available at: https://doi.org/10.1016/j.addma.2021.102203.

Li, R. and Xiong, J. (2019) 'Influence of interlayer dwell time on stress field of thin-walled components in WAAM via numerical simulation and experimental tests', *Rapid Prototyping Journal*, 25(8), pp. 1433–1441. Available at: https://doi.org/10.1108/RPJ-03-2019-0067.

Lundbäck, A. (no date) 'CAD-support for heat input in FE-model', p. 10.

Mohebbi, M.S., Kühl, M. and Ploshikhin, V. (2020) 'A thermo-capillary-gravity model for geometrical analysis of single-bead wire and arc additive manufacturing (WAAM)', *The International Journal of Advanced Manufacturing Technology*, 109(3–4), pp. 877–891. Available at: https://doi.org/10.1007/s00170-020-05647-6.

Mukin, D. *et al.* (2021) 'An Extended Analytical Solution of the Non-Stationary Heat Conduction Problem in Multi-Track Thick-Walled Products during the Additive Manufacturing Process', *Materials*, 14(23), p. 7291. Available at: https://doi.org/10.3390/ma14237291.

Mukin, D., Valdaytseva, E. and Turichin, G. (2021) 'Analytical Solution of the Non-Stationary Heat Conduction Problem in Thin-Walled Products during the Additive Manufacturing Process', *Materials*, 14(14), p. 4049. Available at: https://doi.org/10.3390/ma14144049.

Nunes, A. C. (1983) An Extended Rosenthal Weld Model, Welding Journal - Welding research Supplement, p. 6.

Nguyen, N.T. *et al.* (1999) 'Analytical Solutions for Transient Temperature of Semi-Infinite Body Subjected to 3-D Moving Heat Sources', p. 11.

Ren, K. *et al.* (2020) 'Thermal field prediction for laser scanning paths in laser aided additive manufacturing by physics-based machine learning', *Computer Methods in Applied Mechanics and Engineering*, 362, p. 112734. Available at: https://doi.org/10.1016/j.cma.2019.112734.

Viola R. S. et al. (2021) 'Complex interaction between CMT equipment and robot controllers during the WAAM process: consequences for toolpath accuracy, *Journal of Robotics and computer-integrated Manufacturing'*, (Submitted in 17/12/2021)

Wolfer, A.J. *et al.* (2019) 'Fast solution strategy for transient heat conduction for arbitrary scan paths in additive manufacturing', *Additive Manufacturing*, 30, p. 100898. Available at: https://doi.org/10.1016/j.addma.2019.100898.

Wu, B. *et al.* (2018) 'A review of the wire arc additive manufacturing of metals: properties, defects and quality improvement', *Journal of Manufacturing Processes*, 35, pp. 127–139. Available at: https://doi.org/10.1016/j.jmapro.2018.08.001.